14. Bergmeyer, H. U. *Methods of Enzymatic Analysis* (Verlag Chemie, Weinheim/Bergstr., 1974).

15. Kushnir, M. M., Komaromy-Hiller, G., Shushan, B., Urry, F. M. & Roberts, W. L. Analysis of dicarboxylic acids by tandem mass spectrometry. High-throughput quantitative measurement of methylmalonic acid in serum, plasma, and urine. *Clin. Chem.* **47,** 1993–2002 (2001).

16. Martin, M., Ferrier, B. & Baverel, G. Transport and utilization of alpha-ketoglutarate by the rat kidney *in vivo. Pflugers Arch.* **413,** 217–224 (1989).

17. Gullans, S. R., Kone, B. C., Avison, M. J. & Giebisch, G. Succinate alters respiration, membrane potential, and intracellular K$^+$ in proximal tubule. *Am. J. Physiol.* **255,** F1170–F1177 (1988).

18. Gullans, S. R., Brazy, P. C., Dennis, V. W. & Mandel, L. J. Interactions between gluconeogenesis and sodium transport in rabbit proximal tubule. *Am. J. Physiol.* **246,** F859–F869 (1984).

19. Krebs, H. A. Rate control of the tricarboxylic acid cycle. *Adv. Enzyme Regul.* **8,** 335–353 (1970).

20. Hems, D. A. & Brosnan, J. T. Effects of ischaemia on content of metabolites in rat liver and kidney *in vivo. Biochem. J.* **120,** 105–111 (1970).

21. Pan, L. *et al.* Critical roles of a cyclic AMP responsive element and an E-box in regulation of mouse renin gene expression. *J. Biol. Chem.* **276,** 45530–45538 (2001).

22. Hackenthal, E., Paul, M., Ganten, D. & Taugner, R. Morphology, physiology, and molecular biology of renin secretion. *Physiol. Rev.* **70,** 1067–1116 (1990).

23. An, S. *et al.* Identification and characterization of a melanin-concentrating hormone receptor. *Proc. Natl Acad. Sci. USA* **98,** 7576–7581 (2001).

24. Brandish, P. E., Hill, L. A., Zheng, W. & Scolnick, E. M. Scintillation proximity assay of inositol phosphates in cell extracts: high-throughput measurement of G-protein-coupled receptor activation. *Anal. Biochem.* **313,** 311–318 (2003).

25. Chuang, P. T., Kawcak, T. & McMahon, A. P. Feedback control of mammalian Hedgehog signaling by the Hedgehog-binding protein, Hip1, modulates Fgf signaling during branching morphogenesis of the lung. *Genes Dev.* **17,** 342–347 (2003).

26. Palczewski, K. *et al.* Crystal structure of rhodopsin: A G protein-coupled receptor. *Science* **289,** 739–745 (2000).

27. Krege, J. H., Hodgin, J. B., Hagaman, J. R. & Smithies, O. A noninvasive computerized tail-cuff system for measuring blood pressure in mice. *Hypertension* **25,** 1111–1115 (1995).

28. Sugiyama, F. *et al.* QTL associated with blood pressure, heart rate, and heart weight in CBA/CaJ and BALB/cJ mice. *Physiol. Genomics* **10,** 5–12 (2002).

29. Silva, A. P. *et al.* Bilateral nephrectomy delays gastric emptying of a liquid meal in awake rats. *Ren. Fail.* **24,** 275–284 (2002).

30. Woronicz, J. D., Gao, X., Cao, Z., Rothe, M. & Goeddel, D. V. IκB kinase-β: NF-κB activation and complex formation with IκB kinase-α and NIK. *Science* **278,** 866–869 (1997).

....

Aquaporin-0 membrane junctions reveal the structure of a closed water pore

Tamir Gonen[1], **Piotr Sliz**[2], **Joerg Kistler**[3], **Yifan Cheng**[1] & **Thomas Walz**[1]

[1]*Department of Cell Biology, Harvard Medical School, 240 Longwood Avenue, Boston, Massachusetts 02115, USA*

[2]*Howard Hughes Medical Institute and Children's Hospital Laboratory of Molecular Medicine, 320 Longwood Avenue, and Department of Biological Chemistry and Molecular Pharmacology, Harvard Medical School, 240 Longwood Avenue, Boston, Massachusetts 02115, USA*

[3]*School of Biological Sciences, University of Auckland, Auckland PO Box 92019, New Zealand*

The lens-specific water pore aquaporin-0 (AQP0) is the only aquaporin known to form membrane junctions *in vivo*[1]. We show here that AQP0 from the lens core, containing some carboxy-terminally cleaved AQP0[2,3], forms double-layered crystals that recapitulate *in vivo* junctions. We present the structure of the AQP0 membrane junction as determined by electron crystallography. The junction is formed by three localized interactions between AQP0 molecules in adjoining membranes, mainly mediated by proline residues conserved in AQP0s from different species but not present in most other aquaporins. Whereas all previously determined aquaporin structures show the pore in an open conformation[4–9], the water pore is closed in AQP0 junctions. The water pathway in AQP0 also contains an additional pore constriction, not seen in other known aquaporin structures[4–9], which may be responsible for pore gating.

AQP0 is a member of the aquaporin family, members of which form pores that are either highly selective for water (aquaporins) or also permeable to other small neutral solutes such as glycerol (aquaglyceroporins) (reviewed in ref. 10). To date, the atomic structures of three aquaporins have been determined (AQP1[4–6], GlpF[7,8] and AQPZ[9]). Sequence alignment shows AQP0 to be closely related to the pure water channel AQP1 (43.6% identity, 62.6% similarity). The presence of His 172, a residue conserved only in aquaporins but substituted in aquaglyceroporins, also suggests that AQP0 forms a pure water pore. AQP0 water permeability at neutral pH is approximately 40 times lower than that of AQP1[11], but AQP0 water conductance doubles under mildly acidic conditions[12]. In the case of aquaporins in plant roots, a pH-dependent closure of the water pores has been reported[13]. Thus, evidence suggests that certain aquaporin pores are gated.

AQP0 water pores are considered essential for the lens micro-circulation system, proposed to supply deeper-lying fibre cells with nutrients and to clear waste products[14,15]. Unlike all other aquaporins, AQP0 is also present in membrane junctions. It is particularly enriched in the 11–13 nm thin junctions between lens fibre cells, that feature square AQP0 arrays[1]. Atomic force microscopy analysis of *in vitro* reconstituted AQP0 two-dimensional crystals demonstrated these crystals to be double-layered[16].

Using AQP0 from the core of sheep lenses, where some of the AQP0 is proteolytically cleaved near the C terminus at various sites in an age-dependent manner[2,3], we reproduced the double-layered two-dimensional crystals[16,17]. When core AQP0 was reconstituted at a lipid-to-protein ratio of 0.25 (w/w), large membrane sheets formed ($>6\,\mu$m) that in some cases showed two parallel edges, revealing them to be double-layered (Fig. 1a). The crystals showing $p422$ symmetry had lattice constants of $a = b = 65.5$ Å and a thickness of 11 nm (Fig. 2a), the same dimensions as thin junctions in the lens[1]. Double-layered AQP0 two-dimensional crystals are therefore likely to recapitulate thin lens fibre cell junctions.

Electron diffraction analysis of AQP0 crystals (tilted to an angle of up to 70°) produced strong diffraction spots to 3 Å resolution in all directions (Fig. 1b, c; the electron crystallographic data are summarized in Table 1). As the crystal structure of the homologous bovine AQP1 was available[5], we determined the structure of the AQP0 membrane junction by molecular replacement, thus avoiding the cumbersome and time-consuming process of collecting high-resolution images of tilted specimens. Sequencing of cloned sheep AQP0 showed an identical amino acid sequence to bovine AQP0[18], with the exception of three conservative (S20T, M90V and S240T) and one non-conservative substitutions (C14F).

Our model (Fig. 2a) shows unique features that enable AQP0 to form membrane junction interactions. These differ from those previously suggested based on atomic force microscopy data[16]. The extracellular surface of AQP0 is rather flat and the interactions are mediated by direct contacts of the corresponding loops in the opposing AQP0 molecules (Fig. 2a). Loop C, connecting α-helices three and four, is significantly shorter than in AQP1 and GlpF. The shortened loop C (also seen in AQP2, AQP5, AQP6 and AQP8) is crucial for the formation of the very tight AQP0 junction, as it allows three specific interactions to be formed that are mediated almost exclusively by proline residues.

The most striking interaction involves Pro 38, in extracellular loop A. The proline residues (Pro 38) from eight symmetry-related AQP0 molecules in the stacked tetramers come together to form a

unique rosette-like structure in the very centre of the junction (Fig. 2b, c). The two other interactions involve three AQP0 molecules that we designated A, B and C (Fig. 2d, e). The contacts are formed by residues in the shortened loop C, namely a Proline–Proline motif (Pro 109 and Pro 110), which is part of a one-turn helix (helix HC), and residues Arg 113 and Pro 123. The proline–proline motif in molecule A, located in the top layer of the junction, interacts with the symmetry-related proline–proline motif of mole-cule C in the bottom layer. Arg 113 in loop C of molecule C is in close proximity with the carbonyl of Pro 123 of B, back in the top layer, making it a likely hydrogen-bonding partner. The connections continue in this way, such that Arg 113 of B interacts with Pro 123 of C, and the proline–proline motif of B interacts with the symmetry-related proline–proline motif in the next AQP0 molecule. Thus, all subunits in interacting AQP0 tetramers are connected to two other subunits in the opposite layer.

In top views, the water pore can readily be seen in AQP1 (Fig. 3a), whereas the AQP0 pore appears much more constricted (Fig. 3b). About half of the residues lining the pores differ between AQP0 and AQP1, and many residues in AQP1 are substituted with larger and more hydrophobic ones in AQP0. The AQP1 pore profile, calculated with the program 'HOLE'[19], shows a single constriction site formed by residues Phe 58, His 182, Arg 197 and Cys 191 (left and middle panel Fig. 3c). This ar/R site (so called because it contains an aromatic and an Arg residue)[20] was arbitrarily chosen as pore height 0. The ar/R site in AQP0 (left and right panel Fig. 3c) is formed by the corresponding residues Phe 48, His 172, Arg 187 and Ala 181, but it shows noteworthy differences. Ala 181 replaces AQP1's Cys 191, thus rendering AQP0 water conductance insensitive to mercurials[21]. His 172 moves towards the centre of the pore compared with AQP1's His 182, resulting in a minimum pore diameter of 1.96 Å, which is too narrow for water permeation. Moreover, the conformation of Arg 187 differs from those of the corresponding arginine residues in the ar/R constriction site in all other aquaporin structures. The distinctive conformation of Arg 187 is stabilized by hydrogen bonds with the backbone carbonyl of Ala 117 and with the side chain of Asn 119 of loop C. Whereas the ar/R constriction in AQP1 is only 1 Å long, constriction site I in AQP0 has a length of approximately 10 Å. The extension of the constriction site towards the extracellular surface (Fig. 3c, pore height 0 to 5 Å) results from the orientation of residues Ser 31 and Met 176 in the extracellular vestibule, whereas the extension of the constriction into the pore (Fig. 3c, pore height 0 to −5 Å) is due to residues Tyr 23, His 172, Asn 184 (part of the NPA motif in loop E) and Gly 182.

The AQP0 pore is also significantly narrower than the AQP1 pore at the site of the NPA motif in the cytoplasmic half of the pore (Fig. 3c, pore height −11 Å), resulting from the side chain of Phe 141 (Leu 151 in AQP1) pointing towards Asn 68 of the NPA motif in loop B.

Constriction site II in the cytoplasmic half of the pore (Fig. 3c, pore height −18 Å) is new. The side chain of Tyr 149 extends into the water pathway and together with Phe 75 and His 66 constricts the pore to a minimum diameter of 2.0 Å, again too narrow for water to pass. It thus seems that on junction formation, AQP0 ceases to function as a water pore. We note, however, that our resolution is
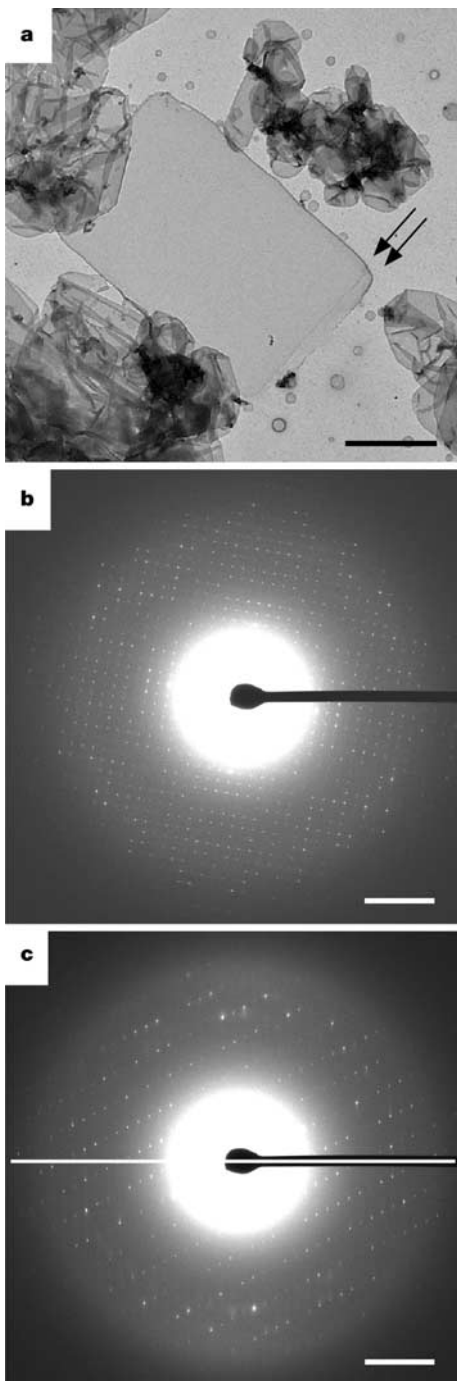

Figure 1 Double-layered two-dimensional crystals of AQP0. **a**, Reconstitution of lens core AQP0 produced large double-layered two-dimensional crystals. The edges of the two layers can be seen (arrows). **b**, Typical electron diffraction pattern of an untilted two-dimensional crystal showing diffraction spots to a resolution of 3 Å. **c**, Representative diffraction pattern of a two-dimensional crystal tilted to 70° showing strong and sharp diffraction spots, even perpendicular to the tilt axis. White line represents the orientation of the tilt axis. Scale bars correspond to 1 μm in **a** and (25 nm)$^{-1}$ in **b** and **c**.

Table 1 **Electron crystallographic data**

Measurement	Value
Two-dimensional crystals	
Layer group	p422
Unit cell	a = b = 65.5 Å
Thickness (assumed)	160 Å
Electron diffraction	
Number of patterns merged	131 (0°, 4; 20°, 12; 45°, 53; 60°, 39; 70°, 23)
Resolution	3.0 Å in membrane plane, 3.5 Å perpendicular to membrane plane
$R_{Friedel}$	15.7%
R_{merge}	16.0% (54% at 3.5–3.0 Å)
Observed amplitudes to 3.0 Å	51,282
Maximum tilt	71.3°
Fourier space sampled	88.1% (82.0% at 3.5–3.0 Å)
Multiplicity	6.7 (4.5 at 3.5–3.0 Å)
Crystallographic refinement	
Crystallographic R-factor	30.20%
Free R-factor	33.85%
Ramachandran plot (%)	81.5/14/4/0.5 (favourable, additional, generous, disallowed)

currently limited to 3 Å, and even if a pore appears to be in a closed conformation, it might still be permeable to solutes[22]. Nonetheless, the length of constriction site I combined with the additional constriction site II makes it unlikely that the AQP0 pore in this conformation has significant water permeability.

Tyrosine 149, part of constriction site II, displays a relatively high *B*-factor, indicative of high mobility. Its hydroxyl group is also not hydrogen bonded and the side chain has sufficient space to change its conformation. It is therefore likely that Tyr 149 can swing out to open the water pore, thus constituting a possible gating mechanism

for the AQP0 pore. AQP0 water permeability is pH-dependent with a maximum at a slightly acidic pH[12]. Two histidine residues, His 40 and His 66, are at positions where they could easily influence water conductance (Fig. 3c). Histidine 40, which has already been implicated in the pH-dependence of AQP0 water conductance[12], is situated right at the extracellular entrance of the pore, and the side chain extends into the water pathway. Histidine 66 is part of constriction site II. It is therefore likely that AQP0 water permeability may be affected by protonation/deprotonation of these two histidines.
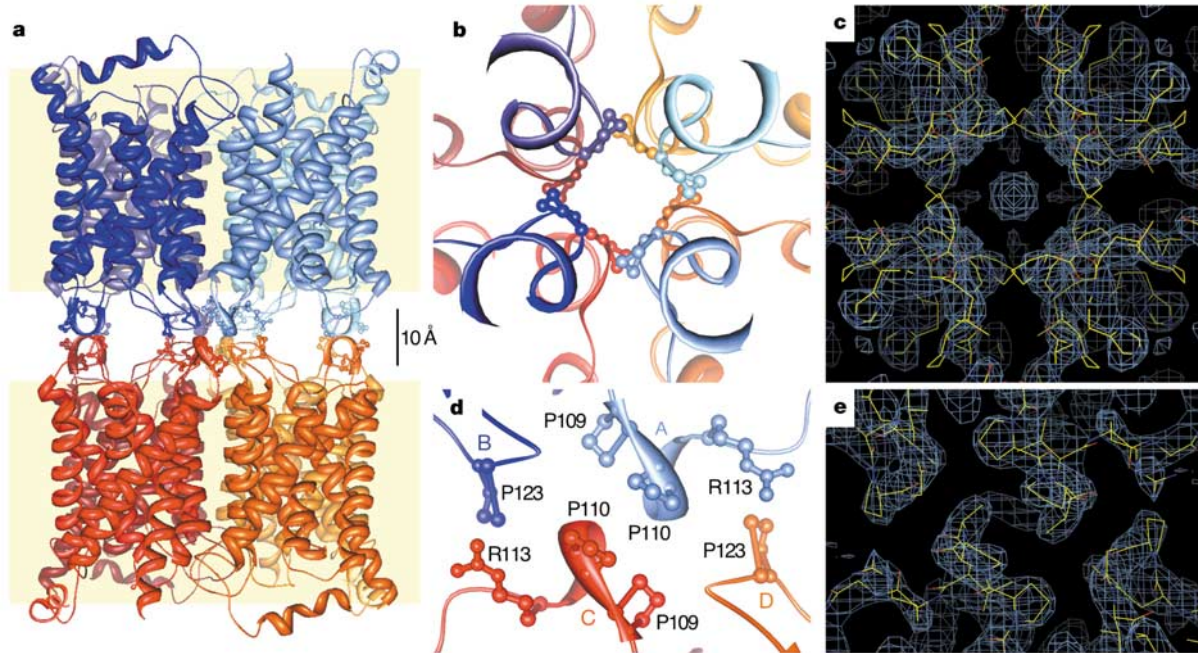

Figure 2 The AQP0-mediated membrane junction. **a**, Ribbon representation of the membrane junction with the positions of the two membranes indicated in yellow. **b**, The Pro 38 residues contributed by all eight AQP0 subunits in the two interacting tetramers. **c**, Corresponding area of the $2F_o–F_c$ map. **d**, The C loops connect each AQP0 molecule to two molecules in the opposite membrane. Letters A to D refer to the molecules described in the text. **e**, Corresponding area of the $2F_o–F_c$ map. Panels **a**, **b** and **d** were created with Chimera[29] and panels **c** and **e** with the program O[28].
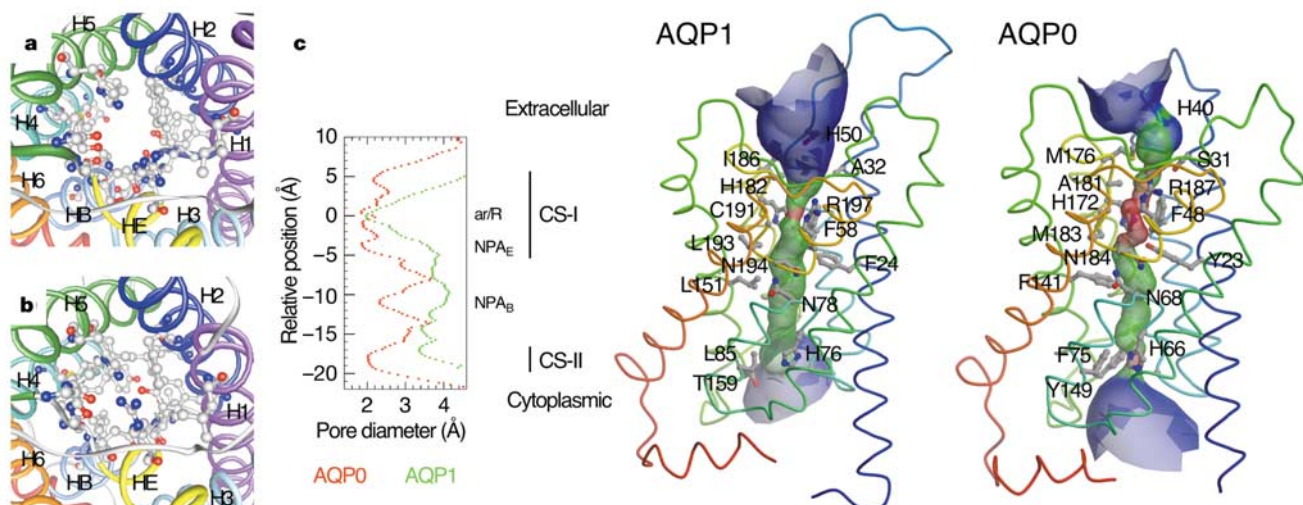

Figure 3 The closed AQP0 water pore. **a**, **b**, Side chains lining the pores in AQP1 (**a**) and AQP0 (**b**). **c**, The left panel shows pore profiles for AQP0 (red) and AQP1 (green) generated with the program 'HOLE'. The positions of the NPA motifs, the ar/R constriction site in AQP1 and the two constriction sites in AQP0 (CS-I, CS-II) are marked and shown in red. The pore profiles are aligned with the models of AQP1 (middle panel) and AQP0 (right panel). Panels **a** and **b** were created with Chimera[29].

AQP0 forms functional water pores[11] with a maximal water conductance around pH 6.5[12]. Our structure of junctional AQP0 determined from two-dimensional crystals produced at pH 6 shows the pore in a closed conformation. We propose that junction formation induces the closed pore conformation in our AQP0 structure. AQP0 and other aquaporins may be in a dynamic equilibrium between an open and a closed water pore conformation, a well-established concept in the ion channel field. Junction formation might then simply stabilize AQP0 in the closed pore conformation, which is otherwise not favoured at pH 6. In this respect, it is notable that the conformation of Arg 187, part of the ar/R constriction site, is stabilized by a hydrogen bond with Asn 119 in loop C, the loop that mediates most of the junction-forming interactions. It is therefore conceivable that junction formation involving residues Pro 109, Pro 110, Arg 113 and Pro 123 in loop C moves Asn 119 into a position in which it can stabilize the alternative conformation of Arg 187. This initial effect would then induce further conformational changes in pore-lining residues ultimately resulting in complete pore closure including Tyr 149 in constriction site II. The structure thus suggests a testable model for the way in which junction formation induces closure of the AQP0 water pore. □

Methods

Sequence of sheep lens AQP0

RNA was isolated from homogenized lens cortical tissue using Trizol (Invitrogen) according to manufacturer's instructions. First strand synthesis was performed using the Superscript first strand synthesis system for polymerase chain reaction with reverse transcription (RT–PCR) (Invitrogen). The synthesized complementary DNA was used for PCR amplification with Taq polymerase (Qiagen) and 1 μM of each sense (5′-CAGGGACCCAGGCGTTGT-3′) and anti-sense (5′-ATGGCAGGAGCAAAGGAG-3′) primers designed using the available sequence for bovine AQP0 (GenBank accession number NM173937). Products were resolved on a 0.8% agarose gel. The DNA was extracted using the quick gel extraction kit (Qiagen) and sequenced at the Harvard Biopolymer facility.

Purification of AQP0

Lenses were dissected to separate the soft cortical tissue from the hard core. Membranes were prepared from the lens core as described[23]. Membranes were solubilized with 1% decyl maltoside (DM) in 10 mM Tris at pH 8, for 30 min at 37 °C, and insoluble material removed by centrifugation at 110,000 g. Proteins were bound to a MonoQ column (Amersham) equilibrated with 0.3% DM in 10 mM Tris at pH 8, and AQP0 eluted with 200 mM NaCl. Pooled fractions were run over a Superose 12 column (Amersham) equilibrated with 0.3% DM in 10 mM Tris at pH 8 and 150 mM NaCl.

Reconstitution of purified lens AQP0 into lipid bilayers

Purified AQP0 was mixed with DM-solubilized dimyristoyl phosphatidyl choline (DMPC) at varying lipid-to-protein ratios. The mixture was placed in a dialysis button and the detergent removed by dialysis against 10 mM MES at pH 6, 50 mM MgCl₂, 150 mM NaCl, 5 mM dithiothreitol and 0.02% NaN₃ at room temperature.

Electron microscopy and data processing

Negatively stained samples, prepared and imaged as described[17], were used to assess the outcome of reconstitution experiments. For cryo-electron microscopy, two-dimensional crystallization samples were mixed with an equal amount of 20% glucose and the suspension applied to molybdenum grids (provided by Y. Fujiyoshi) covered with a thin layer of carbon film. Grids were blotted to remove excess material, loaded onto a high-tilt cryo-transfer holder (Gatan) and transferred into a Philips Tecnai F20 equipped with a field emission electron source and operated at 200 kV. The sample was cooled to the temperature of liquid nitrogen, and low-dose electron diffraction data were recorded with a Gatan 2Kx2K slow-scan CCD camera using a camera length of 3,000 mm and a selected area diffraction aperture of 70 μm. Electron diffraction patters were analysed as described[24].

Molecular replacement and model building

The structure of AQP0 was determined by molecular replacement in MOLREP[25], using as a search model the AQP1 structure[5] lacking amino acid residues 36–47 and 122–134. Crowther fast cross-rotation function calculations identified an orientation of a single subunit in the asymmetric unit as the top solution with an RF signal twice the value of the second peak. The initially determined unit cell axis a = b of 68 Å was refined over ±6 Å in 0.2 Å increments by repeating the search and optimizing the signal. The top solution was identified as 65 Å. The translation function with the monomer in the refined unit cell gave a top solution with an R-factor of 52.5% and a correlation coefficient of 42.7% (average values for the top 50 translation peaks were 57.8% and 25.3%, respectively). In the initial rounds of refinement we evaluated both electron and X-ray scattering factors. As expected for 3 Å resolution data, there was little difference in the resulting refinement statistics[26]. In

all subsequent refinement rounds we used X-ray scattering factors.

At this stage the residues in AQP1 that differed from those in the AQP0 sequence were replaced by alanine (or glycine if the substitution was to glycine). The model was refined using CNS version 1.1 (ref. 27). In a first step the rigid body refinement was repeated, varying the unit cell dimension in 0.2 Å increments. The R-free minimum showed that the cell axis had to be adjusted to 65.5 Å, and this value was used in further refinements. Subsequent model building was performed with the program O (ref. 28) using 2F_o−F_c density modified by solvent flipping (see Supplementary Fig. 1), and simulated annealing composite omit-maps. The model was refined by simulated annealing with a number of refinement parameters (starting temperature, cooling rate, stereochemical weight term, energy constant of dihedral restraints for α-helical regions and range around restrained angles for helical regions) optimized by running several refinement cycles with a wide range of starting values and ultimately selecting the ones that gave the best R-free. Calculations were performed on the HMS structural biology Linux grid. The final refinement statistics are presented in Table 1.

1. Costello, M. J., McIntosh, T. J. & Robertson, J. D. Distribution of gap junctions and square array junctions in the mammalian lens. *Invest. Ophthalmol. Vis. Sci.* **30,** 975–989 (1989).
2. Takemoto, L., Takehana, M. & Horwitz, J. Covalent changes in MIP26K during aging of the human lens membrane. *Invest. Ophthalmol. Vis. Sci.* **27,** 443–446 (1986).
3. Roy, D., Spector, A. & Farnsworth, P. N. Human lens membrane: comparison of major intrinsic polypeptides from young and old lenses isolated by a new methodology. *Exp. Eye Res.* **28,** 353–358 (1979).
4. Murata, K. *et al.* Structural determinants of water permeation through aquaporin-1. *Nature* **407,** 599–605 (2000).
5. Sui, H., Han, B. G., Lee, J. K., Walian, P. & Jap, B. K. Structural basis of water-specific transport through the AQP1 water channel. *Nature* **414,** 872–878 (2001).
6. Ren, G., Reddy, V. S., Cheng, A., Melnyk, P. & Mitra, A. K. Visualization of a water-selective pore by electron crystallography in vitreous ice. *Proc. Natl Acad. Sci. USA* **98,** 1398–1403 (2001).
7. Fu, D. *et al.* Structure of a glycerol-conducting channel and the basis for its selectivity. *Science* **290,** 481–486 (2000).
8. Tajkhorshid, E. *et al.* Control of the selectivity of the aquaporin water channel family by global orientational tuning. *Science* **296,** 525–530 (2002).
9. Savage, D. F., Egea, P. F., Robles-Colmenares, Y., O'Connell, J. D. III & Stroud, R. M. Architecture and selectivity in aquaporins: 2.5 Å X-ray structure of aquaporin Z. *PLoS Biol.* **1,** 334–340 (2003).
10. Agre, P. *et al.* Aquaporin water channels–from atomic structure to clinical medicine. *J. Physiol. (Lond.)* **542,** 3–16 (2002).
11. Chandy, G., Zampighi, G. A., Kreman, M. & Hall, J. E. Comparison of the water transporting properties of MIP and AQP1. *J. Membr. Biol.* **159,** 29–39 (1997).
12. Nemeth-Cahalan, K. L. & Hall, J. E. pH and calcium regulate the water permeability of aquaporin 0. *J. Biol. Chem.* **275,** 6777–6782 (2000).
13. Tournaire-Roux, C. *et al.* Cytosolic pH regulates root water transport during anoxic stress through gating of aquaporins. *Nature* **425,** 393–397 (2003).
14. Mathias, R. T., Rae, J. L. & Baldo, G. J. Physiological properties of the normal lens. *Physiol. Rev.* **77,** 21–50 (1997).
15. Donaldson, P., Kistler, J. & Mathias, R. T. Molecular solutions to mammalian lens transparency. *News Physiol. Sci.* **16,** 118–123 (2001).
16. Fotiadis, D. *et al.* Surface tongue and groove contours on lens MIP facilitate cell-to-cell adherence. *J. Mol. Biol.* **300,** 779–789 (2000).
17. Hasler, L. *et al.* Purified lens major intrinsic protein (MIP) forms highly ordered tetragonal two-dimensional arrays by reconstitution. *J. Mol. Biol.* **279,** 855–864 (1998).
18. Gorin, M. B., Yancey, S. B., Cline, J., Revel, J. P. & Horwitz, J. The major intrinsic protein (MIP) of the bovine lens fiber membrane: characterization and structure based on cDNA cloning. *Cell* **39,** 49–59 (1984).
19. Smart, O. S., Goodfellow, J. M. & Wallace, B. A. The pore dimensions of gramicidin A. *Biophys. J.* **65,** 2455–2460 (1993).
20. de Groot, B. L. & Grubmuller, H. Water permeation across biological membranes: mechanism and dynamics of aquaporin-1 and GlpF. *Science* **294,** 2353–2357 (2001).
21. Varadaraj, K. *et al.* The role of MIP in lens fiber cell membrane transport. *J. Membr. Biol.* **170,** 191–203 (1999).
22. Bond, P. J., Faraldo-Gomez, J. D. & Sansom, M. S. OmpA: a pore or not a pore? Simulation and modeling studies. *Biophys. J.* **83,** 763–775 (2002).
23. Gonen, T., Donaldson, P. & Kistler, J. Galectin-3 is associated with the plasma membrane of lens fiber cells. *Invest. Ophthalmol. Vis. Sci.* **41,** 199–203 (2000).
24. Mitsuoka, K. *et al.* The structure of bacteriorhodopsin at 3.0 Å resolution based on electron crystallography: implication of the charge distribution. *J. Mol. Biol.* **286,** 861–882 (1999).
25. Vagin, A. & Teplyakov, A. An approach to multi-copy search in molecular replacement. *Acta Crystallogr. D* **56,** 1622–1624 (2000).
26. Grigorieff, N., Ceska, T. A., Downing, K. H., Baldwin, J. M. & Henderson, R. Electron-crystallographic refinement of the structure of bacteriorhodopsin. *J. Mol. Biol.* **259,** 393–421 (1996).
27. Brunger, A. T. *et al.* Crystallography & NMR system: A new software suite for macromolecular structure determination. *Acta Crystallogr. D* **54,** 905–921 (1998).
28. Jones, T. A., Zou, J. Y., Cowan, S. W. & Kjeldgaard, M. Improved methods for building protein models in electron density maps and the location of errors in these models. *Acta Crystallogr. A* **47,** 110–119 (1991).
29. Huang, C. C., Couch, G. S., Pettersen, E. F. & Ferrin, T. E. Chimera: an extensible molecular modeling application constructed using standard components. *Pacif. Symp. Biocomput.* **1,** 724 (1996).

....

The GTPase-activating protein Rap1GAP uses a catalytic asparagine

Oliver Daumke[*], **Michael Weyand**[*], **Partha P. Chakrabarti**, **Ingrid R. Vetter & Alfred Wittinghofer**

Max-Planck-Institut für Molekulare Physiologie, Otto-Hahnstr. 11, 44227 Dortmund, Germany

[*] These authors contributed equally to this work

....

Rap1 is a Ras-like guanine-nucleotide-binding protein (GNBP) that is involved in a variety of signal-transduction processes[1,2]. It regulates integrin-mediated cell adhesion and might activate extracellular signal-regulated kinase. Like other Ras-like GNBPs, Rap1 is regulated by guanine-nucleotide-exchange factors (GEFs) and GTPase-activating proteins (GAPs). These GAPs increase the slow intrinsic GTPase reaction of Ras-like GNBPs by many orders of magnitude and allow tight regulation of signalling. The activation mechanism involves stabilization of the catalytic glutamine of the GNBP and, in most cases, the insertion of a catalytic arginine of GAP into the active site[3]. Rap1 is a close homologue of Ras but does not possess the catalytic glutamine essential for GTP hydrolysis in all other Ras-like and Gα proteins. Furthermore, RapGAPs are not related to other GAPs and apparently do not use a catalytic arginine residue[4]. Here we present the crystal structure of the catalytic domain of the Rap1-specific Rap1GAP at 2.9 Å. By mutational analysis, fluorescence titration and stopped-flow kinetic assay, we demonstrate that Rap1GAP provides a catalytic asparagine to stimulate GTP hydrolysis. Implications for the disease tuberous sclerosis are discussed.

Rap1GAP (663 amino acids, molecular mass of 73 kDa) is the founding member of a family of GAPs specific for Rap1[5], and a sequence of 340 amino acids within it is sufficient for Rap1GAP activity[4,6]. Homologous sequences have been identified in human genes *SPA1* (ref. 7), *E6TP1* (ref. 8) and *TSC2*, which encodes tuberin[9]. RapGAPs are thought to be important for tumour suppression because degradation of the E6TP1 protein via the transforming papilloma virus protein E6 correlates with development of cervical cancer[10]. Deletion of the *Spa1* gene in mouse creates a spectrum of myeloid disorders that resemble chronic myeloid leukaemia[11]. Furthermore, mutations in the GAP domain of the tumour suppressor tuberin, a GAP for the Ras-like protein RheB, can cause the benign tumour phenotype tuberous sclerosis[9].

We solved the structure of the catalytic domain of Rap1GAP (residues 75–415)[4,6] by X-ray crystallography to a resolution of 2.9 Å, with an R_{work} of 23.2% and an R_{free} of 27.6% (see Methods, Supplementary Tables 1 and 2). Out of four molecules constituting two dimers (molecule A–B and molecule C–D) in the asymmetric unit, three are well defined in the electron density (molecules A, B

and C). Because no major difference was observed between molecules A and C (root-mean-square deviation 0.5 Å for the Cα atoms), the dimer A–B will be described here. Dimerization was also observed in size-exclusion chromatography in which Rap1GAP elutes with an apparent molecular mass of ∼100 kDa. The size of the dimer interface is approximately 2,400 Å² and is formed mainly by hydrophobic residues.

Each monomer consists of two domains, which we call the dimerization and the catalytic domain. Both domains have an α–β fold, with a central β-sheet surrounded by α-helices (Fig. 1a, Supplementary Fig. 1). Remarkably, the carboxy-terminal catalytic domain shows structural similarity to the G domain of Ras superfamily proteins (Fig. 1b, Supplementary Fig. 2). Its long C-terminal helix, α9, folds back onto the amino-terminal dimerization domain. Because no extensive interaction is observed between the two domains we assume that their relative orientation is variable in solution. Residues outside the catalytic domain are much less conserved, and tuberin does not show any homology to the dimerization domain (Supplementary Fig. 1). Rap1GAP has no structural similarity to GAPs of Ras, Rho, Arf, Rab or Ran[3].

To investigate the role of dimerization, we replaced two hydrophobic residues from the mostly hydrophobic dimerization interface with large polar residues. The resulting mutant (F100E, L173E), which is less stable than the wild-type protein, eluted primarily as a monomer in size-exclusion chromatography (data not shown). In a standard multiple turnover assay (excess Rap1·GTP compared with Rap1GAP, see Methods), this mutant had nearly wild-type activity (Fig. 2). This indicates that dimerization is not required for Rap1GAP activity.

As the sequence of the catalytic domain is more conserved than that of the dimerization domain (Supplementary Fig. 1) and contains two lysines essential for Rap1GAP activity[4], we asked whether the catalytic domain alone is sufficient for Rap1GAP activity. However, constructs containing the core or a more extended catalytic domain were either insoluble or inactive (data not shown). This implies that both domains are necessary for GAP function. Because helix α9 interacts with the dimerization domain, we asked whether helix α9 supports Rap1GAP activity. Figure 2 shows that mutation of the invariant, surface-exposed Arg 388 in helix α9 (Fig. 1c) decreases Rap1GAP activity (see also ref. 4).

Mutations of the highly invariant lysine residues Lys 194 and Lys 285 reduce Rap1GAP activity by 25-fold and 100-fold, respectively, by primarily affecting the affinity for Rap1·GTP[4]. Contrary to expectation, neither of the lysines is exposed to solvent but instead involved in polar interactions that apparently stabilize the structural integrity around helix α7 (Fig. 1c). Lys 194 interacts with Asp 291 and Asn 290, which are residues of helix α7 that are conserved in the Rap1GAP family. Lys 285 of helix α7 makes contacts with the invariant Glu 207 and Ala 310. If the role of Lys 194 and Lys 285 is to position helix α7, then mutation of their contact residues should have a similar effect on catalysis (or binding). This is indeed confirmed by alanine mutations of Glu 207, Asp 291 and His 267, which reduce Rap1GAP activity depending on the loss of their hydrogen-bonding interactions (Fig. 2). The network of interactions described for Lys 194 and Lys 285 is only found in Rap1GAP monomers A and C, indicating a certain flexibility of helix α7 that might be relevant for the catalytic process. All the mutants described above show a drastically reduced affinity for Rap1 that is too low to be measured by either direct binding or multiple turnover K_m measurements. In common with the lysine mutants[4], the major (and maybe exclusive) effect of these mutations is a reduction in affinity between Rap1·GTP and Rap1GAP.

We reasoned that the ionic interactions described above stabilize and position the putative interaction helix α7, which in turn might contain one or more residues essential for catalysis. The solvent-

197